# Chemically imaging nanostructures formed by the covalent assembly of molecular building blocks on a surface with ultrahigh vacuum tip-enhanced Raman spectroscopy

Jeremy F. Schultz<sup>1,\*</sup>, Linfei Li<sup>1</sup>, Sayantan Mahapatra<sup>1</sup>, and Nan Jiang<sup>1,\*</sup>

<sup>1</sup>Department of Chemistry, University of Illinois Chicago, Chicago, Illinois 60607, United States.

\*E-mail: schult36@uic.edu

\*E-mail: njiang@uic.edu

Received xxxxxx Accepted for publication xxxxxx Published xxxxxx

### Abstract

Surface-bound reactions have become a viable method to develop nanoarchitectures through bottom-up assembly with near atomic precision. However, the bottom-up fabrication of nanostructures on surfaces requires careful consideration of the intrinsic properties of the precursors and substrate as well as the complex interplay of any interactions that arise in the heterogenous 2D system. Therefore, it becomes necessary to consider these systems with characterization methods sensitive to such properties with suitable spatial resolution. Here, low temperature ultrahigh vacuum scanning tunneling microscopy (STM) and tip-enhanced Raman spectroscopy (TERS) were used to investigate the formation of 2D covalent networks via coupling reactions of tetra(4-bromophenyl)porphyrin (Br<sub>4</sub>TPP) molecules on a Ag(100) substrate. Through the combination of STM topographic imaging and TERS vibrational fingerprints the conformation of molecular precursors on the substrate was understood. Following the thermally activated coupling reaction, STM and TERS imaging confirm the covalent nature of the 2D networks and suggest that the apparent disorder arises from molecular flexibility.

Keywords: scanning tunneling microscopy, tip-enhanced Raman spectroscopy, 2D covalent networks, binding conformations, surface chemistry

# 1. Introduction

The realization of atomically precise nanostructures through bottom-up assembly necessitates an understanding of the forces that drive their formation [1]. At interfaces (*i.e.*, surfaces), these heterogeneous systems provide a canvas to carefully design and tune fundamental interactions and

chemistry to develop unique and novel low-dimensional nanostructures [2]. The intrinsic properties of molecular building blocks, as well as the surface, along with the interplay between them determine the viability of using rational design principles and chemistry to form new nanoarchitectures [3]. These structures can be stabilized by and formed through a number of interactions, including van der Waals forces,

coordination bonds, hydrogen bonds, halogen—halogen bonds and even covalent bonds through deliberate on-surface chemistry [4]. The situation becomes further complicated when the molecular building blocks are structurally flexible, and molecular binding conformations can be highly affected by molecule—substrate interactions [5]. Although principles of rational design can inform the selection of precursor molecules and substrate, ultimately the system must be understood with analytical techniques that provide insight into the complex interactions that may arise on the surface with respect to highly localized effects.

On metal surfaces, aryl halides can undergo the thermally activated dissociation of C-X bonds leading to the formation of a new coupling C-C bond or the formation of organometallic species [6]. The reaction pathway strongly depends upon the nature of the molecule, substrate, and their interaction. As a result, despite the robust nature of the Ullmann-like coupling reaction, molecular precursors are typically selected based primarily upon their compatiblity with the fabrication method, not necessarily functionality, somewhat limiting its applications [7]. Functional molecules that have found extensive use in metalorganic frameworks or covalent organic frameworks can have substantial molecule-substrate interactions that lead to undesirable binding conformations and therefore prevent methods that rely on bottom-up assembly [1, 8]. And so it becomes necessary to investigate these systems with characterization methods that can provide chemical information with a high enough degree of spatial resolution to capture these potentially atomic-scale phenomena.

The scanning tunneling microscope (STM) provides the necessary spatial resolution to probe nanostructures with respect to highly localized effects [9]. However, the characterization of the products of reactions at the singlemolecule level remains challenging. In fact, early methods to identify the formation of a coupling covalent bond between two molecules on a surface involved dragging one molecule across the surface and observing the second to move as well due to the covalent bond that linked them [3, 10] More recently, new scanning probe microscopy methods have been used to identify the skeletal structures of reaction products [11, 12]. Alternatively, spectroscopic methods can provide chemical information, but due to the diffraction limit of light are restricted to ensemble-based measurements and thus cannot capture defects or other such local phenomena. By bringing Raman spectroscopy into the near field, tip-enhanced Raman spectroscopy (TERS) enables the full characterization of molecules and low-dimensional materials at the subnanoscale [13-15]. It is especially sensitive to intermolecular interactions [16-18], binding conformations [19-22], molecule-substrate interactions [23, 24], and even chemistry at the single-bond level [25-27], resulting in an ideal

tool to consider the interactions and reactions that drive the formation of 2D covalent networks on surfaces [28].

Here we have applied ultrahigh vacuum (UHV) low temperature (LT) STM-TERS to the study of tetra(4bromophenyl)porphyrin (Br<sub>4</sub>TPP) molecules on a Ag(100) substrate. Br<sub>4</sub>TPP consists of four phenyls located at the meso positions of a porphyrin macrocycle with bromine atoms bonded to the carbons at the para position of each phenyl (figure 1a). This results in conformational flexibility within both the porphyrin macrocyle and the respective  $\sigma$  bonds that connect each phenyl to the central macrocycle (figure 1b) [29-321. Due to this conformational flexibility, molecule-substrate interactions become paramount to the realization of wellordered covalent networks. We considered the surfaceactivated coupling reaction of Br<sub>4</sub>TPP molecules on a Ag(100) substrate, where the fourfold symmetry and identity of the silver substrate was expected to influence the formation of covalent networks, as shown with an illustration in figure 1c. Ultimately, the combination of STM and TERS imaging at the subnanoscale provided topographic and spectroscopic characterization of the precursor molecules and 2D covalent networks at the subnanoscale.

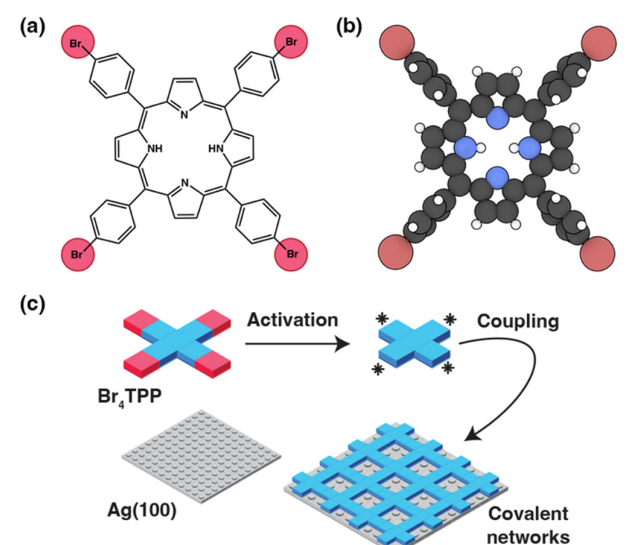


**Figure 1.** Structure of molecular building blocks and proposed realization of 2D covalent networks on Ag(100). (a) Chemical structure of a tetra(4-bromophenyl)porphyrin (Br<sub>4</sub>TPP) molecule. (b) 3D structure of the expected gas phase conformation of a Br<sub>4</sub>TPP molecule. (c) Proposed formation of covalently bound networks by coupling thermally activated molecular building blocks (Br<sub>4</sub>TPP) on the Ag(100) substrate. The active sites of the intermediate species form through the dissociation of C–Br bonds and are noted with asterisks in the illustration.

### 2. Methods

Experiments took place in a variable temperature (VT) scanning probe microscope (SPM) system (UNISOKU Co., Ltd.) in UHV at a base pressure of  $5.0 \times 10^{-11}$  Torr. The

Ag(100) single crystal (Princeton Scientific, 99.999% purity) was prepared in a preparation chamber with a base pressure of  $1.0 \times 10^{-10}$  Torr. The Ag(100) substrate was cleaned by cycles of argon ion sputtering and indirect thermal annealing to 800 K. The tetra(4-bromophenyl)porphyrin (Br<sub>4</sub>TPP) molecules were purchased from Frontier Scientific and deposited via a Knudsen cell style molecular evaporator (315°C) to obtain sub-monolayer coverage. To deposit Br<sub>4</sub>TPP onto a low-temperature substrate, the substrate was first held at  $\sim 78 \, K$  in the STM then quickly transferred to the preparation chamber to perform the vapor deposition. Following this time ( $\sim 2-3$  minutes), the sample was immediately returned to the low-temperature sample stage for STM and TERS measurements. These measurements all took place at liquid nitrogen temperature ( $\sim$ 78 K). The STM was operated in constant current mode with the bias applied to the sample with respect to the grounded tip. Ag tips, prepared with an electrochemical etching process [33], were used for STM imaging and TERS experiments. The STM operation was controlled with Nanonis SPECS electronics. The Raman spectral mapping was carried out through a synchronization function between the STM controller and CCD camera. Gwyddion was used to process STM images [34].

A 561 nm solid-state continuous-wave laser (LASOS) polarized parallel to the tip was used as the excitation source for TERS experiments. The incident laser power was maintained at 500 µW for all TERS spectra. Most optical elements were mounted in separate cage systems outside of the UHV chamber with the important exception of the *invacuo* lenses positioned near the tip to allow for an optimal laser spot focus and collection efficiency. An Isoplane SCT-320 spectrometer coupled with a PIXIS 100 CCD (Princeton Instruments) was used for TERS measurements. The spectra were processed with a combination of Python and MATLAB by adapting established methods [35].

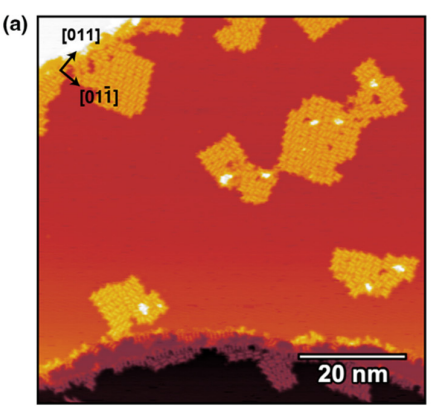
# 3. Results and Discussion

Due to the expected reactivity of the C–Br bonds within Br<sub>4</sub>TPP molecules on the Ag(100) substrate, the molecules were first deposited onto a precooled substrate as previously described. As shown in the STM image in figure 2a, Br<sub>4</sub>TPP molecules formed self-assembled molecular islands with no isolated molecules visible on the Ag(100) substrate under these conditions.

This initial observation suggests a few preliminary conclusions regarding the behavior of  $Br_4TPP$  molecules on the Ag(100) surface relevant to the eventual formation of 2D covalent networks. First, although the deposition was carried out below room temperature, the  $Br_4TPP$  molecules still self-assembled to form molecular islands, revealing a relatively weak molecule–substrate interaction [36]. This is further supported by the absence of any isolated bromine atoms on the surface that would occur due to the surface-catalyzed

dissociation of aromatic C–Br bonds [5, 37-39]. However, despite the apparent weak nature of the molecule–substrate interactions, the roughly rectangular molecular islands appear to adopt one of two possible orientations on the surface based on the angle of the island edges relative to the close-packed directions of the (100) substrate.

With the high degree of spatial resolution inherent to the STM, it becomes possible to develop an understanding of molecule-substrate interactions at the single-molecule level. The STM image in figure 2b reveals the orientation of individual Br<sub>4</sub>TPP molecules within a molecular island relative to the atomic lattice of the surface. Although the STM topography corresponds to the Local Density of States (LDOS) and not necessarily the actual topography [40], the apparent molecular structures suggest that the molecules adopt the so-called "saddle-shape" conformation. In this conformation, opposing macrocyclic pyrrole rings tilt by the same angle and the peripheral phenyls located at the meso positions rotate about their respective  $\sigma$  bonds to the macrocycle [41-43]. Crucially, as is visible in the STM images, the potential fourfold symmetry of the molecule becomes reduced to twofold symmetry in this binding conformation. Due to the orientation of the peripheral phenyl rings, the terminal bromine atoms lie parallel to the substrate and the apparent supramolecular assemblies appear to be mediated in part by halogen-halogen bond interactions [44-47]. However, the accurate assignment of molecular conformations typically relies upon spectroscopy. Traditionally, this has been accomplished with techniques such as near edge x-ray absorption fine structure analysis and photoelectron spectroscopy among others [48-50].



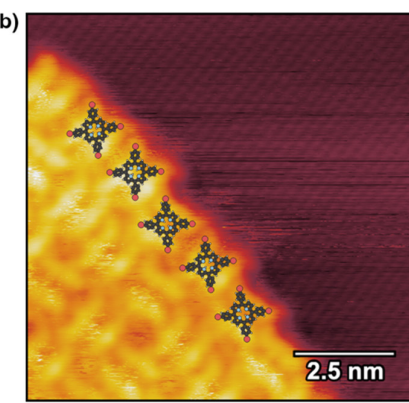


**Figure 2.** STM images of Br<sub>4</sub>TPP on the Ag(100) substrate. (a) Large-scale STM image of the self-assembled molecular islands of Br<sub>4</sub>TPP that form following vapor deposition onto a precooled Ag(100) substrate (U = +1.0 V, I = 100 pA). (b) Zoomed-in STM image of Br<sub>4</sub>TPP molecules with atomic resolution of the adjacent surface (U = +1.0 V, I = 100 pA). Scaled molecular models are overlaid.

While such traditional spectroscopic methods provide vibrational fingerprints of molecular ensembles, due to the diffraction limit of light, they cannot capture vibrational fingerprints at the single-molecule level. In contrast, by bringing optical spectroscopy into the near-field, TERS can provide single-molecule and in some cases even intramolecular spatial resolution [13-15]. Figure 3 presents the TERS vibrational fingerprint that corresponds to a Br<sub>4</sub>TPP molecule adsorbed on the Ag(100) substrate. The analysis of this spectrum benefits from the relatively extensive study of other tetraphenylporphyrin derivatives that adopt saddled conformations on a surface with TERS [20, 21, 51, 52]. Figure 3a is a TERS spectrum that corresponds to a Br<sub>4</sub>TPP molecule located within a molecular island on a terrace, where the conformation expected based on STM imaging appears adjacent in figure 3b. The most intense peak located at 1555 cm<sup>-1</sup> can be identified as a vibration within the pyrroles that pull out of the porphyrin plane in the saddled molecule, while the other noticeable vibrational modes, especially those located near 1600 cm<sup>-1</sup>, largely consist of C-C stretching within the phenyl rings [52, 53]. Notably, the peak located at 1074 cm<sup>-1</sup> can be attributed to a phenyl ring vibrational mode that is highly sensitive to the position of halogen substitution based upon a previous Raman study of halogenated TPP [54]. Here, the observed peak confirms that the bromine substituents are at the *para* positions of the phenyl rings and the C–Br bonds are intact. Alongside STM topographic imaging, the TERS vibrational fingerprint provides spectroscopic characterization of the binding conformation of Br<sub>4</sub>TPP molecular precursors on the Ag(100) substrate. As a result, it was possible to develop an understanding of molecule–substrate interactions, setting the stage for the investigation of their effects on the coupling reactions.

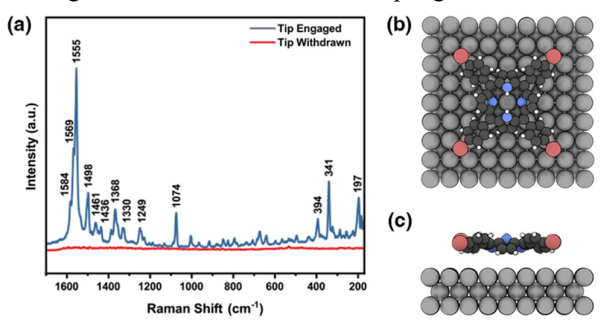


**Figure 3.** TERS vibrational fingerprint for a Br<sub>4</sub>TPP molecule on Ag(100) with a corresponding model. (a) TERS spectra while the tip was positioned over a Br<sub>4</sub>TPP molecule within a molecular island  $(U = +1.0 \text{ V}, I = 100 \text{ pA}, t_{acq} = 3 \text{ s})$ . (b) Top-down view of the saddled binding conformation of a Br<sub>4</sub>TPP molecule on Ag(100) based on STM and TERS studies that corresponds to the spectrum shown in (a). (c) Sideview of the same molecule, illustrating the C–Br bonds that lie parallel to the substrate in this conformation.

Following the STM and TERS characterization of the precursor Br<sub>4</sub>TPP molecules on the Ag(100) surface, the sample was warmed up to and equilibrated at room temperature before being returned to the low-temperature STM head for further measurements. STM imaging reveals a pronounced change, suggesting that the Ullmann-like coupling reaction has occurred. As can be seen in figure 4, the surface is now dotted with bromine atoms that remain adsorbed on the surface following the dissociation of C-Br bonds within the Br<sub>4</sub>TPP molecules [39]. Additionally, the density of the molecular islands is substantially decreased as they now appear to be semi-ordered porous arrays, an effect that can be explained by the formation of coupling bonds resulting in 2D networks [4, 7]. Furthermore, bias-dependent STM imaging reveals the delocalization of the electronic structure (figure 4b), as well as the presence of two organometallic species located within the area marked by the dashed blue square and illustrated with a model in the inset. This identification is based on the apparent contrast difference established for STM images of Ag adatoms that have been incorporated into molecules during the course of Ullmann-like coupling reactions [39, 55]. The final observation is the presence of a few molecules with different bias-dependent contrasts, appearing dimmer at a positive applied bias (figure 4a) and brighter at a negative applied bias (figure 4b). There are two such noticeable species at the top of the array in the STM image. Previously, this has been attributed to a different binding conformation, specifically an inverted conformation for a tetraphenylporphyrin molecule [3, 29, 31], where the relative fourfold symmetry of the molecule is reduced to twofold due to strong molecule-substrate interactions that lead to distortion of the porphyrin macrocycle and phenyl rings. Here, molecules in this conformation were found to disrupt the formation of 2D networks, instead favoring headon interactions that lead to more 1D dimensional chains [56]. Fortunately, this inverted conformation rarely appears on the Ag(100) surface and only appears to occur at temperatures that also induce the Ullmann-like coupling reaction, as no molecules were observed in an inverted confomation with deposition onto the precooled substrate. This observation suggests that the saddled binding conformation is essential to the formation of 2D covalent networks on the surface.

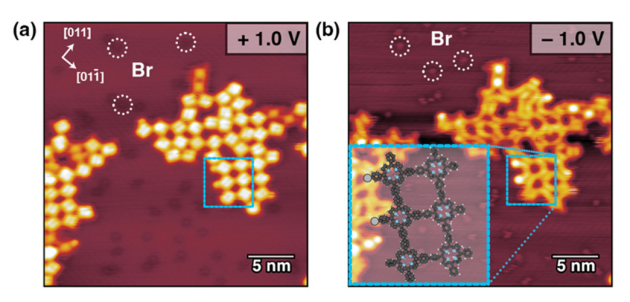


**Figure 4.** Products that form on the surface after the sample prepared by vapor depositing Br<sub>4</sub>TPP molecules onto the precooled Ag(100) substrate was allowed to warm up to room temperature. (a) STM image acquired with a positive applied bias (U = +1.0 V, I = 100 pA). (b) STM image of the same area acquired with a negative applied bias (U = -1.0 V, I = 100 pA). A model of the species within the area designated with a dashed blue square is inset.

Although pre-cooling the Ag(100) substrate allowed the characterization of precursor Br<sub>4</sub>TPP molecules, it was found to not be necessary for the growth of 2D covalent polymer networks. As shown in figure 5a and b, again with biasdependent STM imaging, the deposition of Br<sub>4</sub>TPP molecules onto a room temperature surface led to the dissociation of C-Br bonds and the formation of molecular networks. Bromine atoms can be seen dotting the surface and the molecular networks show the reduced density representative of coupling reactions. Although the networks show some apparent disorder, regions of fourfold symmetric arrays are visible. Furthermore, these molecular networks remain stable on the surface even following progressive thermal annealings beginning at 100°C (figure 5c and d) and through 300°C. Additionally, the bromine atoms found to remain adsorbed on the surface throughout this process.

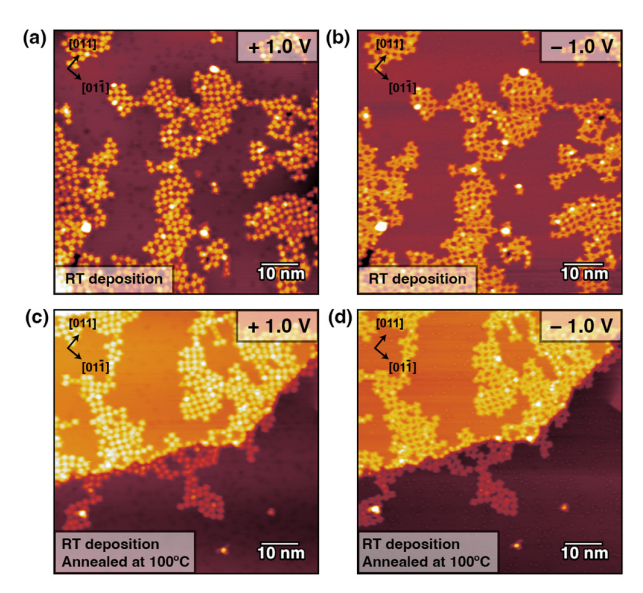


**Figure 5.** STM images of reactions products that form on the surface following the vapor deposition of Br<sub>4</sub>TPP molecules onto a room temperature Ag(100) substrate and slight thermal annealing. (a) STM image acquired with a positive bias of the deposition of Br<sub>4</sub>TPP molecules onto a room temperature Ag(100) substrate (U = +1.0 V, I = 100 pA). (b) STM image of the same area acquired with a negative applied bias (U = -1.0 V, I = 100 pA). (c) STM image acquired with a positive bias following a 10-minute thermal annealing at  $100^{\circ}\text{C}$  (U = +1.0 V, I = 100 pA). (d) STM image of the same area acquired with a negative bias (U = -1.0 V, U = 100 pA).

STM studies of the reaction products were supplemented with the chemical imaging capabilities of TERS to develop an understanding of the nature of the interactions or bonds that result in the formation of the observed porous networks. Figure 6a shows a molecular network that was considered with TERS. Based upon the bias-dependent STM imaging of other molecular networks shown in figures 4 and 5, we propose that the molecular array is stabilized by the formation of covalent bonds between molecules (figure 6b). However, the TERS spectrum of a molecular network shown in figure 6c provides spectroscopic evidence of the covalent bonds that couple phenyl groups of adjacent molecules. The vibrational

fingerprint of the molecular network shows significant differences when compared to a TERS spectrum of a precursor Br<sub>4</sub>TPP molecule. Based on previous Raman studies, the intense and narrow peaks now observed at 1582 cm<sup>-1</sup> and 1319 cm<sup>-1</sup>, highlighted with yellow, can reasonably be assigned to inter-ring C–C stretching between the biphenyl species that now couple porphyrin macrocycles and vibrations of the sp<sup>2</sup> carbons in the phenyl rings [57, 58]. By acquiring sequential TERS spectra in an array and then tracking these specific vibrational modes with curve fitting, it was possible to generate a TERS image of these vibrational modes where the peak areas are plotted in real space as shown in figure 6d and

e. Importantly, due to the stability of the 2D covalent networks on the surface it was possible to bring the tip closer to the surface during spectral acquisition compared to measurements of the precursor molecules where the tip–sample distance was kept larger to avoid disturbing the molecules. This can further confine the enhanced near-field [14] and here provides the ability to spectroscopically identify the covalent bonds that stabilize the molecular networks with nanoscale spatial resolution. As shown in figure 6f, tracking the 1580 cm<sup>-1</sup> and 1320 cm<sup>-1</sup> modes reveals the formation of covalent bonds within the observed networks.

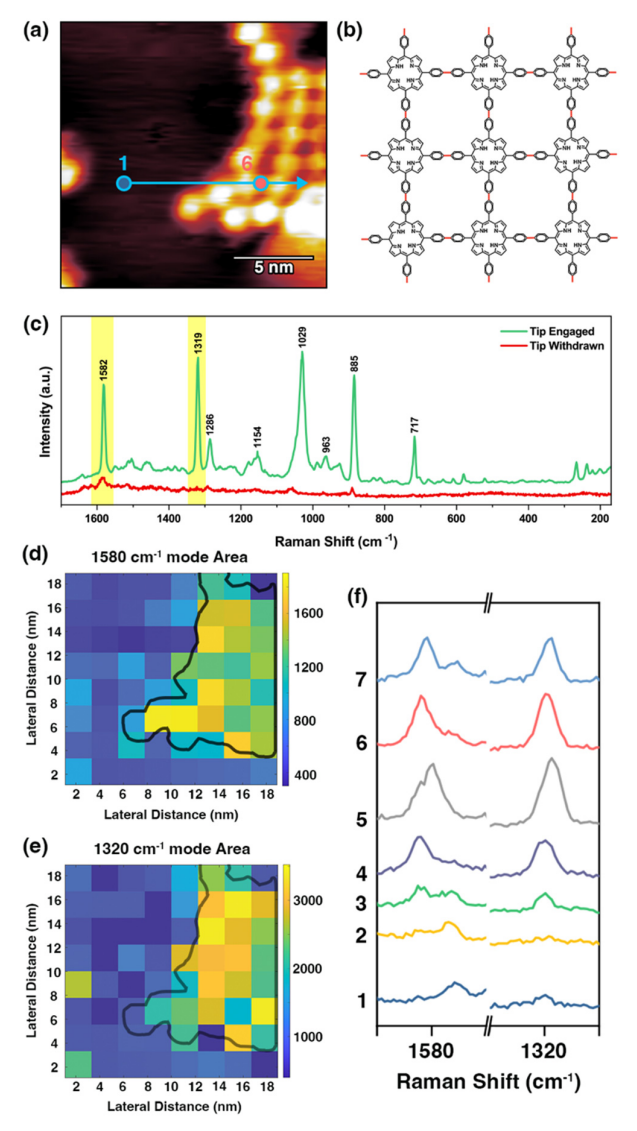


**Figure 6.** STM and a TERS spectrum and imaging of a covalent network formed from the coupling reactions of Br<sub>4</sub>TPP molecules. (a) STM image of a molecular network that was imaged with TERS with an arrow denoting the position and direction of extracted TERS spectra shown in (f) (U = +1.0 V, I = 100 pA). (b) Proposed structure of the molecular network, highlighting the covalent bonds that form between precursor molecules. (c) A sample TERS spectrum

acquired while the tip was positioned over a molecular network ( $U=+100~\rm mV$ ,  $I=2~\rm nA$ ,  $t_{acq}=3~\rm s$ ). The vibrational modes used for TERS imaging are highlighted in yellow. (d) and (e) TERS images acquired based on tracking the area of a curve fit to the 1580 cm<sup>-1</sup> (d) or 1320 cm<sup>-1</sup> (e) vibrational modes across the area shown in (a) with the outline of the network observed in the STM image superimposed ( $U=+100~\rm mV$ ,  $I=2~\rm nA$ ,  $t_{acq}=3~\rm s$  per pixel, 8 pixels × 8 pixels). (f) The spectral evolution of the 1580 cm<sup>-1</sup> and 1320 cm<sup>-1</sup> modes across the arrow shown in (a). Acquisition parameters were the same as described in (d,e), spectra were acquired at 2.5 nm intervals.

Figure 7 shows TERS imaging maps with higher resolution of two other 2D covalent networks, providing further insight into their complicated structure. By considering a smaller array (figure 7a), the 1580 cm<sup>-1</sup> vibrational mode, which corresponds to inter-ring C-C stretching, was found to be more localized to the molecular network (figure 7b). As a result, it was possible to identify a triangular substructure in the top left corner of the small covalent network. Despite the fourfold symmetry of the precursor molecule, distortion in the molecular conformation leads to a triangular oligomer here [31]. Meanwhile, the 1320 cm<sup>-1</sup> mode representative of the phenyl groups predictably shows significant intensity at the periphery of the molecular network. These observations of the localization of these vibrational modes further support their earlier assignments that were based on previous Raman studies.

As shown in figure 7d, larger molecular networks exhibit significant disorder. Although the fourfold symmetry of the atomic lattice of the Ag(100) surface matches the targeted symmetry of the 2D covalent network, the reacted Br<sub>4</sub>TPP molecules do not necessarily form well-ordered nanostructures. STM imaging of these structures does not provide sufficient resolution to define the nature of interactions or bonds that result in the disorder. Instead, TERS can be used to evaluate the 2D covalent networks [28, 59]. Here, by tracking the 1580 cm<sup>-1</sup> (figure 7e) and 1320 cm<sup>-1</sup> (figure 7f) modes, it was possible to confirm that even within the disordered phases, covalent bonds link most monomers. Additionally, by interpreting these TERS images alongside the STM topography, individual defects where covalent coupling bonds did not form could be identified. Together with the earlier observation of the conformational dependence of the coupling reactions of Br<sub>4</sub>TPP molecules, this suggests that the disorder that arises in these nanostructures is in part the result of conformational flexibility within the molecular structure. There is inherent flexibility in the bond that connects the phenyl rings with the porphyrin macrocycle and distortion of this bond results in alternative products beyond the expected fourfold arrays.

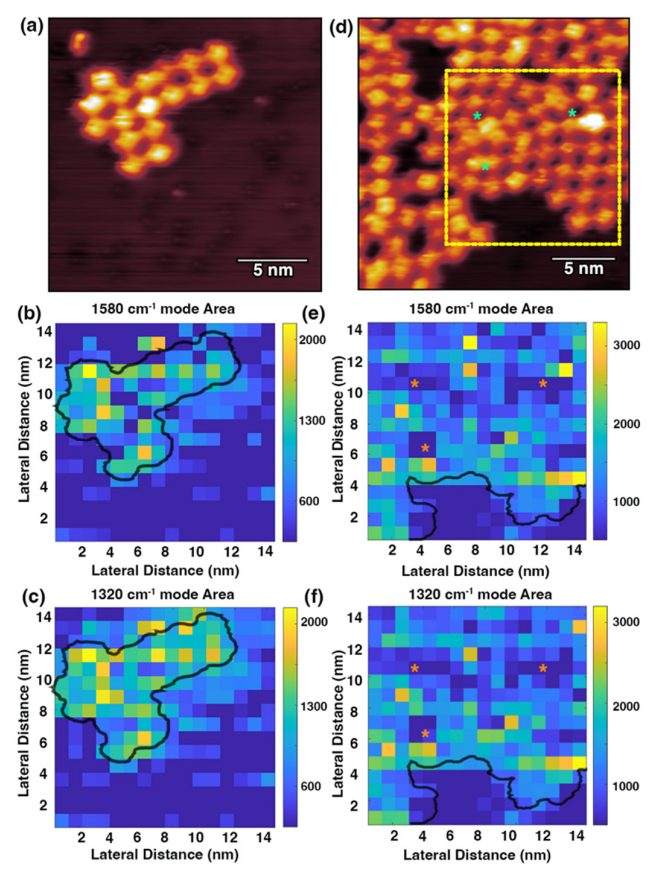


Figure 7. STM and TERS images of two additional covalent networks formed through the coupling reactions of Br<sub>4</sub>TPP molecules. (a) STM image of a small array (U = +1.0 V, I =100 pA). The cyan dashed square marks the area where the below TERS images were acquired. (b) and (c) TERS images acquired based on tracking the area of a curve fit to the 1580 cm<sup>-1</sup> (b) or 1320 cm<sup>-1</sup> (c) peaks across the area shown in (a) with the outline of the network observed in the STM image superimposed (U =+10 mV, I = 2 nA,  $t_{acq} = 3$  s per pixel, 16 pixels × 16 pixels). (d) STM image of a larger molecular network with some disorder evident (U = +1.0 V, I = 100 pA). The yellow dashed square marks the area where the below TERS images were acquired and cyan asterisks note the location of defects. (e) and (f) TERS images acquired based on tracking the area of a curve fit to the 1580 cm<sup>-1</sup> (b) or 1320 cm<sup>-1</sup> (c) peaks across the area shown in (d) with the outline of the network observed in the STM image superimposed. Orange asterisks correspond to the location of defects noted in the STM image ( $U=+10~{\rm mV},~I=2~{\rm nA},~t_{acq}=3~{\rm s}$  per pixel, 16 pixels  $\times$ 16 pixels).

## 3. Conclusions

In conclusion, STM and TERS were used to investigate the 2D covalent networks that form via the coupling reaction of Br<sub>4</sub>TPP molecules on a Ag(100) surface. The binding conformation of molecular precursors was considered with a low-temperature deposition, finding that the C–Br bond lies parallel to the substrate due to a saddled binding conformation,

based on STM imaging and the TERS vibrational fingerprint of an individual molecule. This conformation is favorable towards the formation of covalently coupled arrays. The Ag(100) surface was found to readily catalyze the dissociation of C-Br bonds and result in coupling of monomers at room temperature. The covalent networks that formed were found to be stable on the surface even following thermal annealing to 300°C. STM and TERS imaging were used to characterize the 2D networks, identifying the covalent bonds that form between monomers with subnanoscale spatial resolution. The combination of the two imaging methods provided the ability to identify the presence of defects that arise from a missing coupling covalent bond or disorder that arises from flexibility within a monomer's structure. This work uses topographic and spectroscopic information at the subnanoscale to provide new insight into the complicated interplay of interactions and reactions essential to the realization of nanostructures through bottom-up methods.

# Acknowledgements

The authors acknowledge support from National Science Foundation (CHE-1944796).

### **ORCID iDs**

Jeremy F. Schultz: 0000-0003-2231-6797

Linfei Li: 0000-0002-5217-3005

Sayantan Mahapatra: 0000-0002-7332-196X

Nan Jiang: 0000-0002-4570-180X

### References

- Gates B D, Xu Q, Stewart M, Ryan D, Willson C G and Whitesides G M 2005 New approaches to nanofabrication: Molding, printing, and other techniques Chem. Rev. 105 1171
- [2] Bartels L 2010 Tailoring molecular layers at metal surfaces Nat. Chem. 2 87
- [3] Grill L, Dyer M, Lafferentz L, Persson M, Peters M V and Hecht S 2007 Nano-architectures by covalent assembly of molecular building blocks *Nat. Nanotechnol.* 2 687
- [4] Grill L and Hecht S 2020 Covalent on-surface polymerization Nat. Chem. 12 115
- [5] Li L, Mahapatra S, Liu D, Lu Z and Jiang N 2021 On-surface synthesis and molecular engineering of carbon-based nanoarchitectures ACS Nano 15 3578
- [6] Lackinger M 2017 Surface-assisted Ullmann coupling Chem. Commun. 53 7872
- [7] Lafferentz L, Eberhardt V, Dri C, Africh C, Comelli G, Esch F, Hecht S and Grill L 2012 Controlling on-surface polymerization by hierarchical and substrate-directed growth *Nat. Chem.* 4 215
- [8] Auwarter W, Ecija D, Klappenberger F and Barth J V 2015 Porphyrins at interfaces *Nat. Chem.* 7 105
- [9] Lackinger M and Heckl W M 2011 A STM perspective on covalent intermolecular coupling reactions on surfaces J. Phys. D: Appl. Phys. 44 464011
- [10] Hla S-W, Bartels L, Meyer G and Rieder K-H 2000 Inducing all steps of a chemical reaction with the scanning tunneling

- microscope tip: Towards single molecule engineering *Phys. Rev. Lett.* **85**
- [11] Zhong Q, Ihle A, Ahles S, Wegner H A, Schirmeisen A and Ebeling D 2021 Constructing covalent organic nanoarchitectures molecule by molecule via scanning probe manipulation *Nat. Chem.* 13 1133
- [12] Gross L 2011 Recent advances in submolecular resolution with scanning probe microscopy *Nat. Chem.* 3 273
- [13] Schultz J F, Mahapatra S, Li L and Jiang N 2020 The expanding frontiers of tip-enhanced Raman spectroscopy *Appl. Spectrosc.* 74 1313
- [14] Mahapatra S, Li L, Schultz J F and Jiang N 2020 Tip-enhanced Raman spectroscopy: Chemical analysis with nanoscale to Angstrom scale resolution J. Chem. Phys. 153 010902
- [15] Schultz J F, Li S, Jiang S and Jiang N 2020 Optical scanning tunneling microscopy based chemical imaging and spectroscopy J. Phys.: Condens. Matter 32 463001
- [16] Chiang N, Jiang N, Madison L R, Pozzi E A, Wasielewski M R, Ratner M A, Hersam M C, Seideman T, Schatz G C and Van Duyne R P 2017 Probing intermolecular vibrational symmetry breaking in self-assembled monolayers with ultrahigh vacuum tip-enhanced Raman spectroscopy J. Am. Chem. Soc. 139 18664
- [17] Jiang N, Chiang N, Madison L R, Pozzi E A, Wasielewski M R, Seideman T, Ratner M A, Hersam M C, Schatz G C and Van Duyne R P 2016 Nanoscale chemical imaging of a dynamic molecular phase boundary with ultrahigh vacuum tip-enhanced Raman spectroscopy *Nano Lett.* 16 3898
- [18] Jiang S, Zhang R, Zhang X-B, Zhang Y, Zhang Y and Dong Z-C 2021 Bicomponent supramolecular self-assemblies studied with tip-enhanced Raman spectroscopy J. Raman Spectrosc. 52 366
- [19] Li H, Zhang Y-F, Zhang X-B, Farrukh A, Zhang Y, Zhang Y and Dong Z-C 2020 Probing the deformation of [12]cycloparaphenylene molecular nanohoops adsorbed on metal surfaces by tip-enhanced Raman spectroscopy *J. Chem. Phys.* 153 244201
- [20] Zhang R, Zhang Y, Dong Z C, Jiang S, Zhang C, Chen L G, Zhang L, Liao Y, Aizpurua J, Luo Y, Yang J L and Hou J G 2013 Chemical mapping of a single molecule by plasmonenhanced Raman scattering *Nature* 498 82
- [21] Lee J, Crampton K T, Tallarida N and Apkarian V A 2019 Visualizing vibrational normal modes of a single molecule with atomically confined light *Nature* 568 78
- [22] Schultz J F, Li L, Mahapatra S, Shaw C, Zhang X and Jiang N 2020 Defining multiple configurations of rubrene on a Ag(100) surface with 5 Å spatial resolution via ultrahigh vacuum tipenhanced Raman spectroscopy J. Phys. Chem. C 124 2420
- [23] Whiteman P J, Schultz J F, Porach Z D, Chen H and Jiang N 2018 Dual binding configurations of subphthalocyanine on Ag(100) substrate characterized by scanning tunneling microscopy, tip-enhanced Raman spectroscopy, and density functional theory J. Phys. Chem. C 122 5489
- [24] Li L, Schultz J F, Mahapatra S, Liu X, Shaw C, Zhang X, Hersam M C and Jiang N 2021 Angstrom-scale spectroscopic visualization of interfacial interactions in an organic/borophene vertical heterostructure J. Am. Chem. Soc. 143 15624
- [25] Xu J, Zhu X, Tan S, Zhang Y, Li B, Tian Y, Shan H, Cui X, Zhao A, Dong Z, Yang J, Luo Y, Wang B and Hou J G 2021 Determining structural and chemical heterogeneities of surface species at the single-bond limit Science 371 818
- [26] Zhang C, Jaculbia R B, Tanaka Y, Kazuma E, Imada H, Hayazawa N, Muranaka A, Uchiyama M and Kim Y 2021 Chemical identification and bond control of π-skeletons in a coupling reaction J. Am. Chem. Soc. 143 9461

- [27] Mahapatra S, Ning Y, Schultz J F, Li L, Zhang J-L and Jiang N 2019 Angstrom scale chemical analysis of metal supported trans- and cis-regioisomers by ultrahigh vacuum tip-enhanced Raman mapping *Nano Lett.* 19 3267
- [28] Shao F, Dai W, Zhang Y, Zhang W, Schlüter A D and Zenobi R 2018 Chemical mapping of nanodefects within 2D covalent monolayers by tip-enhanced Raman spectroscopy ACS Nano 12 5021
- [29] Ceccatto dos Santos A, Herrera-Reinoza N, Pérez Paz A, Mowbray D J and de Siervo A 2021 Reassessing the adsorption behavior and on-surface reactivity of a brominated porphyrin on Cu(111) J. Phys. Chem. C 125 17164
- [30] Bischoff F, Riss A, Michelitsch G S, Ducke J, Barth J V, Reuter K and Auwärter W 2021 Surface-mediated ring-opening and porphyrin deconstruction via conformational distortion *J. Am. Chem. Soc.* 143 15131
- [31] Moreno-López J C, Mowbray D J, Pérez Paz A, de Campos Ferreira R C, Ceccatto dos Santos A, Ayala P and de Siervo A 2019 Roles of precursor conformation and adatoms in Ullmann coupling: An inverted porphyrin on Cu(111) Chem. Mater. 31 3009
- [32] Jens B, Mathieu L, Stefan K, Jörg S, Alessandro S, Shih-Hsin C, Germar H, Roland W, Roy L, Paul H J K, Johan H, Alan E R, Martin B, Markus F, Sven S, Francesco Z and Roberto L 2009 Dynamics of molecular self-ordering in tetraphenyl porphyrin monolayers on metallic substrates *Nanotechnology* 20 275602
- [33] Mahapatra S, Li L, Schultz J F and Jiang N 2021 Methods to fabricate and recycle plasmonic probes for ultrahigh vacuum scanning tunneling microscopy-based tip-enhanced Raman spectroscopy J. Raman Spectrosc. 52 573
- [34] Nečas D and Klapetek P 2012 Gwyddion: An open-source software for SPM data analysis Cent. Eur. J. Phys. 10 181
- [35] O'Haver T C 1991 An introduction to signal processing in chemical measurement *J. Chem. Educ.* **68** A147
- [36] Schultz J F and Jiang N 2021 Noble metal substrate identity effects on the self-assembly, dynamics, and dehydrocyclization reaction of octaethylporphyrin molecules J. Phys. Chem. C 125 23680
- [37] Fan Q, Gottfried J M and Zhu J 2015 Surface-catalyzed C-C covalent coupling strategies toward the synthesis of lowdimensional carbon-based nanostructures Acc. Chem. Res. 48 2484
- [38] Schultz J F, Yang B and Jiang N 2020 Direct observation of the geometric isomer selectivity of a reaction controlled via adsorbed bromine *Nanoscale* 12 2726
- [39] Schultz J F, Yang B and Jiang N 2021 On-surface formation of metal-organic coordination networks with C···Ag···C and C=O···Ag interactions assisted by precursor self-assembly J. Chem. Phys. 154 044703
- [40] Tersoff J and Hamann D R 1985 Theory of the scanning tunneling microscope Phys. Rev. B 31 805
- [41] Otsuki J 2010 STM studies on porphyrins Coord. Chem. Rev. 254 2311
- [42] Buchner F, Xiao J, Zillner E, Chen M, Röckert M, Ditze S, Stark M, Steinrück H P, Gottfried J M and Marbach H 2011 Diffusion, rotation, and surface chemical bond of individual 2H-tetraphenylporphyrin molecules on Cu(111) J. Phys. Chem. C 115 24172
- [43] Buchner F, Kellner I, Hieringer W, Görling A, Steinrück H-P and Marbach H 2010 Ordering aspects and intramolecular conformation of tetraphenylporphyrins on Ag(111) Phys. Chem. Chem. Phys. 12 13082

- [44] Clark T, Hennemann M, Murray J S and Politzer P 2007 Halogen bonding: The σ-hole *J. Mol. Model.* **13** 291
- [45] Politzer P, Lane P, Concha M C, Ma Y and Murray J S 2007 An overview of halogen bonding J. Mol. Model. 13 305
- [46] Bui T T T, Dahaoui S, Lecomte C, Desiraju G R and Espinosa E 2009 The nature of halogen···halogen interactions: A model derived from experimental charge-density analysis Angew. Chem. Int. Ed. 48 3838
- [47] Han Z, Czap G, Chiang C-l, Xu C, Wagner P J, Wei X, Zhang Y, Wu R and Ho W 2017 Imaging the halogen bond in self-assembled halogenbenzenes on silver Science 358 206
- [48] Rojas G, Chen X, Bravo C, Kim J-H, Kim J-S, Xiao J, Dowben P A, Gao Y, Zeng X C, Choe W and Enders A 2010 Selfassembly and properties of nonmetalated tetraphenyl-porphyrin on metal substrates J. Phys. Chem. C 114 9408
- [49] Narioka S, Ishii H, Ouchi Y, Yokoyama T, Ohta T and Seki K 1995 XANES spectroscopic studies of evaporated porphyrin films: Molecular orientation and electronic structure *J. Phys. Chem.* 99 1332
- [50] Auwärter W, Seufert K, Klappenberger F, Reichert J, Weber-Bargioni A, Verdini A, Cvetko D, Dell'Angela M, Floreano L, Cossaro A, Bavdek G, Morgante A, Seitsonen A P and Barth J V 2010 Site-specific electronic and geometric interface structure of Co-tetraphenyl-porphyrin layers on Ag(111) Phys. Rev. B 81 245403
- [51] Ghafoor A, Yang B, Yu Y-j, Zhang Y-f, Zhang X-b, Chen G, Zhang Y, Zhang Y and Dong Z-c 2019 Site-dependent TERS study of a porphyrin molecule on Ag(100) at 7 K Chin. J. Chem. Phys. 32 287
- [52] Lee J, Tallarida N, Chen X, Liu P, Jensen L and Apkarian V A 2017 Tip-enhanced Raman spectromicroscopy of Co(II)tetraphenylporphyrin on Au(111): Toward the chemists' microscope ACS Nano 11 11466
- [53] Aydin M 2013 DFT and Raman spectroscopy of porphyrin derivatives: Tetraphenylporphine (TPP) Vib. Spectrosc. 68 141
- [54] Fuchsman W H, Smith Q R and Stein M M 1977 Direct Raman evidence for resonance interactions between the porphyrin ring system and ring-conjugated substituents in porphyrins, porphyrin dications, and metalloporphyrins J. Am. Chem. Soc. 99
- [55] Ammon M, Sander T and Maier S 2017 On-surface synthesis of porous carbon nanoribbons from polymer chains J. Am. Chem. Soc. 139
- [56] Cirera B, de la Torre B, Moreno D, Ondráček M, Zbořil R, Miranda R, Jelínek P and Écija D 2019 On-surface synthesis of gold porphyrin derivatives via a cascade of chemical interactions: Planarization, self-metalation, and intermolecular coupling *Chem. Mater.* 31 3248
- [57] Zhang K and Chen X-J 2019 Identification of the incommensurate structure transition in biphenyl by Raman scattering Spectrochim. Acta, Part A 206 202
- [58] Zhang K and Chen X-J 2018 Chain length effects of poligophenyls with comparison of benzene by Raman scattering AIP Advances 8 025004
- [59] Wang W, Shao F, Kröger M, Zenobi R and Schlüter A D 2019 Structure elucidation of 2D polymer monolayers based on crystallization estimates derived from tip-enhanced Raman spectroscopy (TERS) polymerization conversion data *J. Am. Chem. Soc.* 141 9867